The Excitation of Second Harmonic Poloidal ULF Waves Through Drift-Bounce Resonance With Protons in the Magnetic Dip

Yan Zhuang, Chao Yue, Li Li, Xu-Zhi Zhou, Qiu-Gang Zong, Shan Wang, Ying Liu, Xing-Yu Li, Ze-Fan Yin, Yong-Fu Wang, et al.

JGR Space Physics

RESEARCH ARTICLE
10.1029/2024JA032804

Key Points:

- Van Allen probe B observed drift-bounce resonance between second harmonic poloidal ULF waves and protons in the magnetic dip
- Through finite Larmor radius effects, the ULF waves are found to propagate eastward with an azimuthal wave number in the range of 237–277
- The magnetic dip leads to an enhancement of proton phase space density locally, which provides free energy to generate ULF waves

Correspondence to:
C. Yue,
yuechao@pku.edu.cn

Citation:
Zhuang, Y., Yue, C., Li, L., Zhou, X.-Z., Zong, Q.-G., Wang, S., et al. (2024). The excitation of second harmonic poloidal ULF waves through drift-bounce resonance with protons in the magnetic dip. *Journal of Geophysical Research: Space Physics*, *129*, e2024JA032804. https://doi.org/10.1029/2024JA032804

Received 20 AUG 2024
Accepted 4 NOV 2024
Corrected 19 DEC 2024

This article was corrected on 19 DEC 2024. See the end of the full text for details.

The Excitation of Second Harmonic Poloidal ULF Waves Through Drift-Bounce Resonance With Protons in the Magnetic Dip

Yan Zhuang[1], Chao Yue[1], Li Li[1], Xu-Zhi Zhou[1], Qiu-Gang Zong[1,2], Shan Wang[1], Ying Liu[1], Xing-Yu Li[1], Ze-Fan Yin[1], Yong-Fu Wang[1], Zhi-Yang Liu[3], and Haobo Fu[1]

[1]Institute of Space Physics and Applied Technology, Peking University, Beijing, China, [2]State Key Laboratory of Lunar and Planetary Sciences, Macau University of Science and Technology, Taipa, China, [3]IRAP, CNES-CNRS-Universite Toulouse III Paul Sabatier, Toulouse, France

Abstract The drift-bounce resonance between ultralow-frequency (ULF) waves and charged particles is an efficient way to transfer energy. In this study, we report the excitation of ULF waves through drift-bounce resonance with protons in the magnetic dip for the first time. On 4 September 2015, Van Allen probe B observed ULF signals with a frequency of ∼10 mHz inside the magnetic dip during substorms at the dusk side. The ULF waves are further diagnosed as second harmonic poloidal waves. The 54–67 keV protons in the magnetic dip exhibit oscillations with the same period as ULF waves, providing evidence for drift-bounce resonance. Through finite Larmor radius effects, we determined that the ULF waves propagate eastward with an azimuthal wave number in the range of 237–277. The ULF waves are excited with free energy related to the enhanced proton phase space density in the magnetic dip.

Plain Language Summary During substorms, energetic particles are injected from the magnetotail to the inner magnetosphere. The magnetic dip, generated by the diamagnetic motion of the injected particles, may further influence the particles therein. On 4 September 2015, Van Allen probe B encountered a magnetic dip at dusk during a substorm event. Inside the magnetic dip, the fields oscillate quasi-periodically, and the protons of 54–67 keV show corresponding perturbations, which reveal drift-bounce resonance between protons in the magnetic dip and ULF waves. We found the waves propagate eastward with a short azimuthal wavelength. Further investigation determined for the first time that the ring current protons inside the magnetic dip provide free energy for the ULF wave generation through drift-bounce resonance.

1. Introduction

During substorms, particles are injected from the magnetotail. In the source region, sudden enhancements of fluxes in different energies are detected by satellites, which are known as dispersionless injections (Birn et al., 1997; Motoba et al., 2021; Zhuang et al., 2023). Subsequently, these particles drift around the earth, displaying dispersive features. Driven by injections of ring current ions, magnetic dips which are characterized by a localized magnetic field depression in the inner magnetosphere would be formed due to pressure balance (Ebihara et al., 2008; He et al., 2017; Xiong et al., 2017; Yin et al., 2021; Zhu et al., 2021; Zhuang et al., 2023). Magnetic dips would further have an impact on the particles therein. For example, if the magnetic field depression reaches a sufficient depth, a local minimum in the radial profile of the field strength would be formed, which reverses the radially inward gradient of the background dipole field. As a result, drifting ions moving perpendicular to the magnetic gradient would become trapped in the magnetic dip and maintain the dispersionless structure of ion injections on the front side (Yin et al., 2021). In such cases, even beyond the injection region, at duskside or even at noon, satellites occasionally observe signatures of dispersionless flux enhancements (He et al., 2017; Yin et al., 2021). The magnetic dip would also cause a decrease in relativistic electron fluxes and modulate their pitch angle distributions (e.g., Chen et al., 2022; Xiong et al., 2017). Additionally, the magnetic dips are also favorable for electromagnetic ion cyclotron (EMIC) wave excitation. The relationship between the magnetic dip and EMIC waves has been extensively discussed (He et al., 2017; Huang et al., 2021; Yan et al., 2023; Yin et al., 2022; Zhao et al., 2023) as increasing anisotropy tends to excite EMIC waves (Yin et al., 2022; Yue et al., 2019). However, the wave-particle interactions between particles in the magnetic dip and the ULF waves have not yet been discussed in detail.

The ULF waves, whose frequencies are in the range of 1 mHz −1 Hz, play a crucial role in energy transport through wave-particle interactions. Drift-bounce resonance is one of the efficient ways to exchange energy between particles and ULF waves (Li et al., 2024; Liu et al., 2020; Ren et al., 2016; Yang et al., 2011; Zhu et al., 2020; Zong et al., 2017). According to Southwood and Kivelson (1981), drift-bounce resonance occurs when the following condition is satisfied:

$$\omega - m\omega_d = N\omega_b \tag{1}$$

where ω is the wave angular frequency, m is the azimuthal wave number, ω_d is the particle's bounce-averaged drift frequency, ω_b is the particle's bounce frequency, and N is an integer that represents the number of azimuthal wavelengths the particles drift across within a bounce cycle in the wave rest frame. According to Southwood et al. (1969) and Southwood and Hughes (1983), the energy transfer direction between particles and ULF waves depends on the sign of

$$\frac{df}{dW} = \frac{\partial f}{\partial W}\bigg|_{\mu_{res},L} + \frac{dL}{dW}\frac{\partial f}{\partial L}\bigg|_{\mu_{res},W_{res}} \tag{2}$$

where f is the phase space density, μ_{res} is the magnetic moment of resonant particles, L is the McIlwain's L shell parameter (McIlwain, 1961), and W_{res} is the resonant energy. If $\frac{df}{dW}$ is positive, particles provide a free energy source, leading to the excitation of waves; Conversely, if $\frac{df}{dW}$ is negative, waves are damped, while particles gain energy.

ULF waves can be excited through various means, either externally or internally. External sources such as the Kelvin–Helmholtz (K–H) instability (Claudepierre et al., 2008) and solar wind dynamic pressure pulses or interplanetary shocks (Hao et al., 2014; Li et al., 2022; Xie et al., 2023; Zhang et al., 2020; Zong, 2022; Zong et al., 2009, 2012) can trigger ULF waves. Alternatively, ULF waves may be internally driven by ring current particles (Glassmeier et al., 1999; Hughes et al., 1978; Min et al., 2017; Ozeke & Mann, 2008; Takahashi et al., 2018; Yamamoto et al., 2019). Regarding internal sources, the presence of a positive energy gradient can lead to the excitation of ULF waves. For instance, Glassmeier et al. (1999), Liu et al. (2013), and Takahashi et al. (2018) found that protons with a bump-on-tail structure were responsible for exciting the ULF waves. Additionally, a density gradient resulting in a positive $\frac{dL}{dW}\frac{\partial f}{\partial L}$ can also contribute to the excitation of ULF waves (Min et al., 2017; Yamamoto et al., 2019). For example, Min et al. (2017) pointed out that westward second harmonic poloidal ULF waves with high m number mode are likely driven by an inward radial gradient of ring current protons in the plume region. However, there is currently no reported evidence of the excitation of ULF waves through drift-bounce resonance with protons in the magnetic dip.

In this study, we report observations from Van Allen probes confirming the excitation of eastward second harmonic ULF waves with high azimuthal wave number through drift-bounce resonance with protons in a magnetic dip. The overview of the event, the properties of the waves, and the drift-bounce resonance with protons in the magnetic dip are presented in Section 2.1. The determination of the wave propagation direction and the estimation of azimuthal wave number through finite Larmor radius effects are discussed in Section 2.2. The energy transfer between the protons and the ULF waves is calculated in Section 2.3. Section 3 discusses our findings and outlines the main conclusions. Our study conclusively supports the excitation mechanism of ULF waves related to the enhanced proton phase space density in the magnetic dip.

2. Results

2.1. Overview

In this study, we use proton flux measured by the Radiation Belt Storm Probes Ion Composition Experiment (RBSPICE) instrument (Mitchell et al., 2013), along with electromagnetic field data from the Electric Field and Waves (EFW) instrument (Wygant et al., 2013), and the Electric and Magnetic Field Instrument Suite and Integrated Science (EMFISIS) instrument (Kletzing et al., 2013) on board Van Allen Probes (Mauk et al., 2013), which are also known as Radiation Belt Storm Probes (RBSP). On 4 September 2015, RBSP-B encountered a magnetic dip at dusk side during a substorm with the maximum value of SuperMAG electrojet index (SME_{max})

~1,000 nT. There is no sudden solar wind dynamic pressure pulse before this event. Unfortunately, RBSP-A was in the inner radiation belt during this time and thus missed this event. Figure 1a shows the detrended magnetic field derived by subtracting a background field. Here, the background field is derived from the sum of the field strength in the International Geomagnetic Reference Field (IGRF) model (Thébault et al., 2015) and a 30-min running average of the difference between the magnetic field measured by Van Allen Probes and the field strength in the IGRF model (Yin et al., 2022). As shown, the total magnetic field decreases by approximately 13 nT. Within the magnetic dip, the fields oscillate quasi-periodically. Figures 1b and 1c illustrate magnetic and electric field oscillations in the magnetic mean field-aligned (MFA) coordinates, respectively. The MFA coordinate system is defined as follows: the parallel component ($\mathbf{e}_p$) is the direction of the magnetic field, the azimuthal component ($\mathbf{e}_\phi$) is defined as $\mathbf{e}_\phi = \mathbf{e}_p \times \mathbf{R}$, where $\mathbf{R}$ is the spacecraft position vector relative to the center of the Earth, and radial component ($\mathbf{e}_r$) is given by $\mathbf{e}_r = \mathbf{e}_\phi \times \mathbf{e}_p$. As shown, the radial magnetic component (B_r) displays more significant fluctuations than the azimuthal component (Figure 1b), and the azimuthal electric field's (E_ϕ) amplitude is greater than the radial one (Figure 1c). These observations suggest that poloidal mode ULF wave (Figure 1d) is dominant. In addition, a cross-wavelet analysis (Grinsted et al., 2004) shows E_ϕ leads B_r by 90° (Figure 1e). Given that RBSP-B was positioned in the northern hemisphere, these findings indicate that the observed waves are even harmonic waves (e.g., Liu et al., 2013; Singer et al., 1982). Furthermore, a closer examination through continuous wavelet power spectra of B_r (Figure 1f) and E_ϕ (Figure 1g) reveals that the period of these poloidal ULF waves approximately falls within the range of Pc4 waves (45–150 s), estimated to be around ~100 s. This observation corresponds well with the theoretical eigenperiod for second harmonic poloidal ULF waves derived from the model by Rankin et al. (2020), thereby providing evidence that these ULF waves are second harmonic waves. In conclusion, the ULF waves observed in this event can be characterized as Pc4 second harmonic poloidal waves.

Figure 2 shows the proton flux observations during this event in association with field variations given in Figure 2a. Figure 2b shows the energy-time spectrograms of omnidirectional differential proton fluxes measured by RBSPICE, which exhibit overall enhancement and quasi-periodic oscillations. In particular, the pitch angle-time spectrograms for 54 and 67 keV protons (Figures 2d and 2e) reveal a series of distinct curved stripes, which is more pronounced for 54 keV protons (Figure 2d). However, no clear stripes are visible for protons in 44 keV (Figures 2c) and 81 keV (Figure 2f). To illustrate the flux oscillations more clearly, Figure 2h displays omnidirectional residual flux ($j_{res} = \frac{j - j_0}{j_0}$,where j represents the observed flux and j_0 is a 10-min running average of j). Additionally, Figures 2i and 2j illustrate the residual fluxes of 54 and 67 keV protons. The fluxes oscillate quasi-periodically with the same period as the magnetic and electric fields. Notably, the peaks of the electric field in Figure 2g (marked by dashed vertical lines) correspond to the intensification of the omnidirectional flux and each stripe around 90° in the pitch angle-time spectrograms for 54 and 67 keV protons. Figure 2i shows 180° phase shifts across 40°/140°, suggesting that the resonant pitch angle of 54 keV protons is 40°/140° as expected from the Southwood and Kivelson (1981) theory. The symmetric and anti-symmetric stripes with respect to the 90° pitch angle are signatures of interaction with fundamental and second harmonic ULF waves, respectively. Here, the stripes are asymmetric with respect to the 90° pitch angle, which is a characteristic signature of protons interacting with second harmonic ULF waves, combined with energy and pitch angle mixing. This asymmetry shown in Figures 2i and 2j can be explained by the bounce phase difference between the northward and southward protons as they encounter RBSP-B in the northern hemisphere.

2.2. Estimation of Azimuthal Wave Number

The ULF wave signals are only detected by RBSP-B. Without the facilitation from other nearby satellites, we thus determine the wave propagation direction and the azimuthal wave number (m) through finite Larmor radius effects (Kivelson & Southwood, 1983; Lin et al., 1988; Su et al., 1977) which occur when the characteristic length of the waves is on a comparable scale to the Larmor radius of the particles, resulting in flux oscillations with a phase difference observable between back-to-back particle detectors. This effect has been successfully employed to calculate the azimuthal wave number m (e.g., Min et al., 2017; Takahashi et al., 2018; Yamamoto et al., 2018), with the result consistent with those obtained through two-point measurements (Takahashi et al., 2018).

In Figures 3a and 3b, the local 90° pitch angle proton fluxes are organized in the gyrocenter direction relative to the spacecraft and time. The r−ϕ plane of the MFA coordinates is perpendicular to the ambient magnetic fields. $\mathbf{e}_\phi$ represents the azimuthal direction with +ϕ pointing eastward, and $\mathbf{e}_r$ is the radial direction with +r pointing

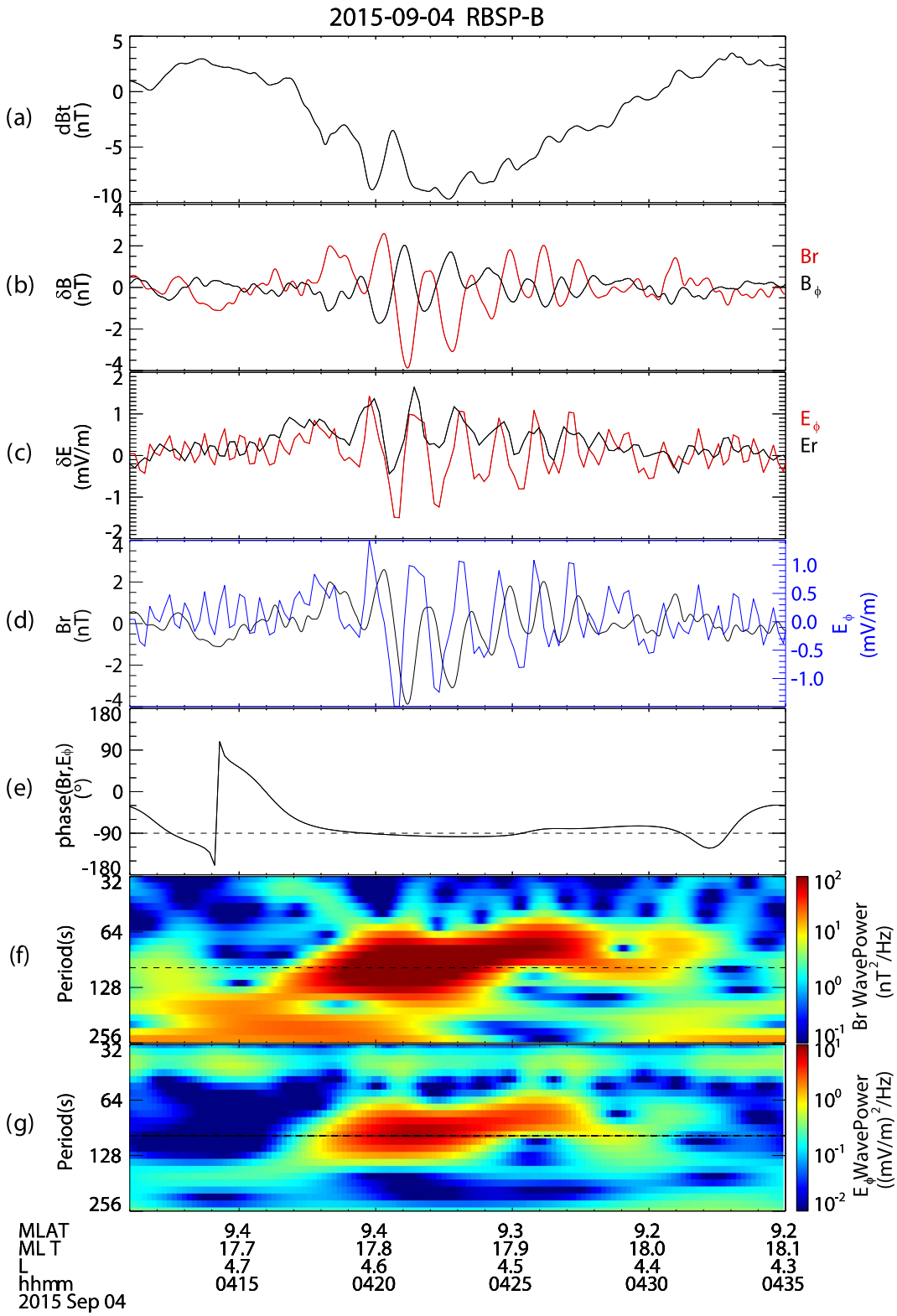

Figure 1.

outward. Regarding the measurements in the r−ϕ plane that are due to the left-handed gyro-motion of protons with respect to a magnetic field along + z, we converted the measured particle direction to the gyrocenter direction. For instance, the fluxes in the +ϕ gyrocenter direction correspond to those measured by the +r direction particle detector (particle velocities in the −r direction), as illustrated in Figure 9a of Takahashi et al. (2018). As shown in Figures 3a and 3b, there is a phase delay between oscillations in the +ϕ and −ϕ gyrocenter direction. The fluxes in the −ϕ direction lead the phase in oscillation, indicating that the wave is propagating in the +ϕ direction (eastward) because protons whose gyrocenters are located westward of the spacecraft are affected by the waves first. Besides, the fluxes in the +r gyrocenter direction are greater than those in the −r direction, indicating an outward gradient of phase space densities (PSD).

Furthermore, we determine the value of m using fluxes in the ϕ direction. Su et al. (1977) obtained the first-order perturbed particle distribution function associated with the waves in a nonuniform magnetic field, subsequently deriving the flux oscillations. If the spacecraft spin period is much shorter than the wave period, and under the assumption of eastward propagating waves, the particle flux oscillations (δj) at a distance of Larmor radius (ρ_G) from the spacecraft due to the waves can be described by the following equation (Kivelson & Southwood, 1983; Min et al., 2017; Su et al., 1977; Yamamoto et al., 2019):

$$\delta j \propto \exp\left[i(\boldsymbol{k}\cdot\mathbf{r_G}-\omega t)\right]=\exp\left[i\left(2\pi\mathbf{e_k}\cdot\frac{\mathbf{r_G}}{\lambda_\phi}-\omega t\right)\right] \tag{3}$$

where $\mathbf{k}$ is the wave vector ($|\mathbf{k}|=\frac{2\pi}{\lambda_\phi}$, where λ_Φ represents azimuthal wavelength), $\mathbf{r_G}$ is a position vector of the guiding center from the spacecraft projected on the plane perpendicular to the ambient magnetic field ($|\mathbf{r_G}|=\rho_G$), $\mathbf{e_k}$ is a unit vector of wave propagation direction, and ω is wave angular frequency. From Equation 3, the phase difference of the flux oscillations between the flux of the eastward guiding center (+ϕ) and that of the westward guiding center (−ϕ) can be expressed by

$$|\delta\theta|=|\delta\theta_{east}-\delta\theta_{west}|=\frac{2\pi\cdot 2\rho_G}{\lambda_\phi} \tag{4}$$

in which

$$\lambda_\phi=\frac{2\pi R_C}{|m|} \tag{5}$$

where R_C is the projection to the magnetic equatorial plane of the radial distance between the center of the Earth and the position of the spacecraft. Combining Equations 4 and 5, the m can be obtained by:

$$|m|=\frac{R_C}{2\rho_G}|\delta\theta| \tag{6}$$

Besides, the phase delay ($|\delta\theta|$) could be derived through the time delay (τ) between fluxes in the +ϕ and −ϕ directions, which is expressed by:

$$|\delta\theta|=\omega\tau=2\pi f\tau \tag{7}$$

where f is wave frequency. Therefore, m can be expressed by the following equation:

Figure 1. The waves observed by RBSP-B on 4 September 2015 inside a magnetic dip. From top to bottom are (a) variations of the total magnetic field strength, (b) radial (red) and azimuthal (black) components of the magnetic field in the MFA coordinates, (c) azimuthal (red) and radial (black) component of the electric field in the MFA coordinates, (d) the radial magnetic component B_r (black) and the azimuthal component of electric field E_ϕ (blue), (e) phase difference between B_r and E_ϕ, and the horizontal dashed line denotes −90° (f)–(g) Continuous wavelet power spectrum of radial magnetic field (f) and azimuthal electric field (g). The horizontal dashed lines in (f) and (g) denote the period of 100s.

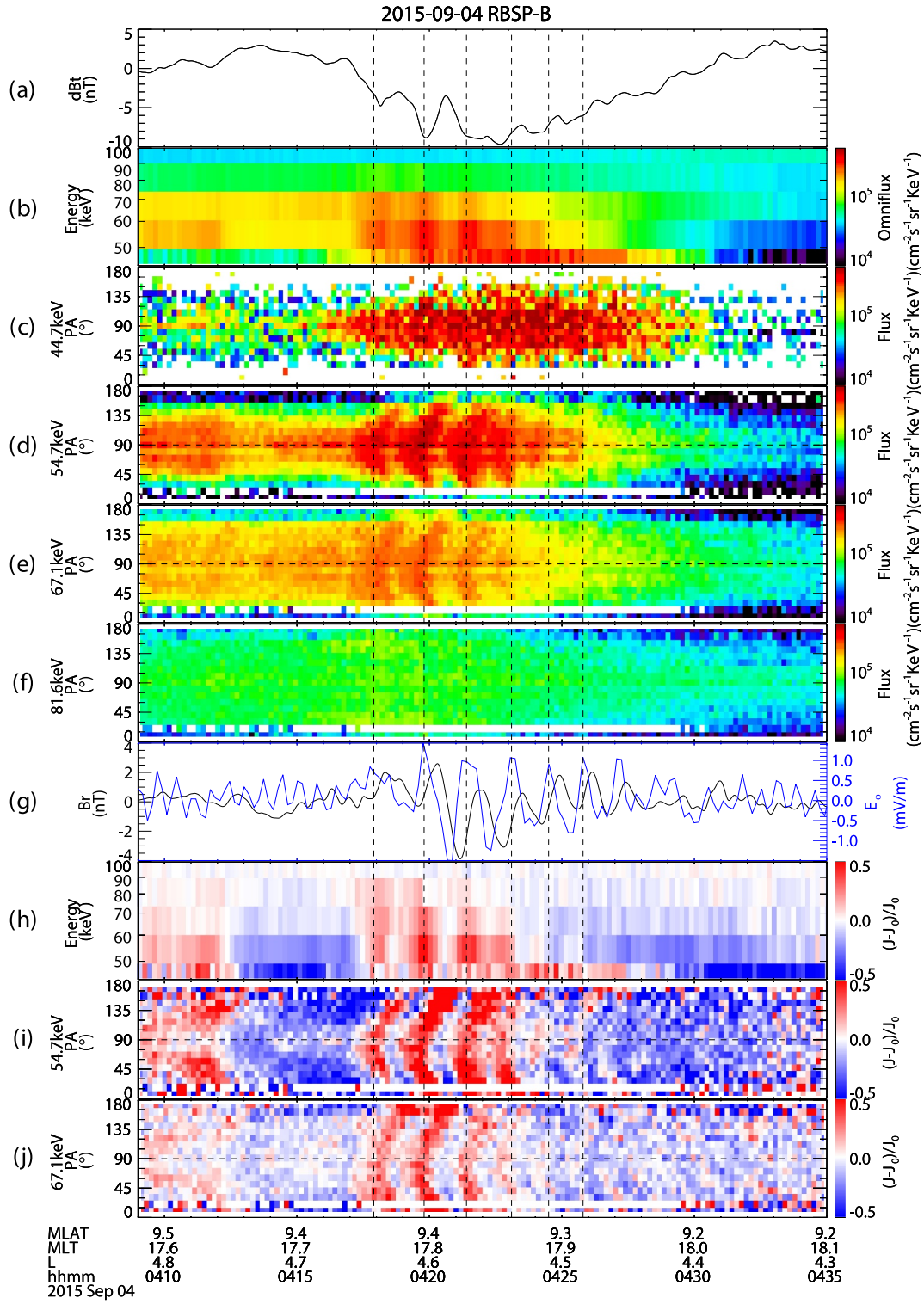

Figure 2. The wave-particle interactions during this event. From top to bottom are (a) variations of the total magnetic field strength, (b) energy spectrum of omnidirectional differential proton fluxes measured by RBSPICE, (c)–(f) pitch-angle distributions of proton fluxes from 44 to 81 keV measured by RBSPICE, (g) the radial magnetic component B_r (black) and the azimuthal component of electric field E_ϕ (blue), (h) the energy spectrum of residual omnidirectional differential proton flux, (i) pitch-angle distributions of residual proton fluxes in 54 keV (j) pitch-angle distributions of residual proton fluxes in 67 keV. The vertical dashed lines indicate the maximum of E_ϕ in (g) as well as each curved stripe in (i) and (j).

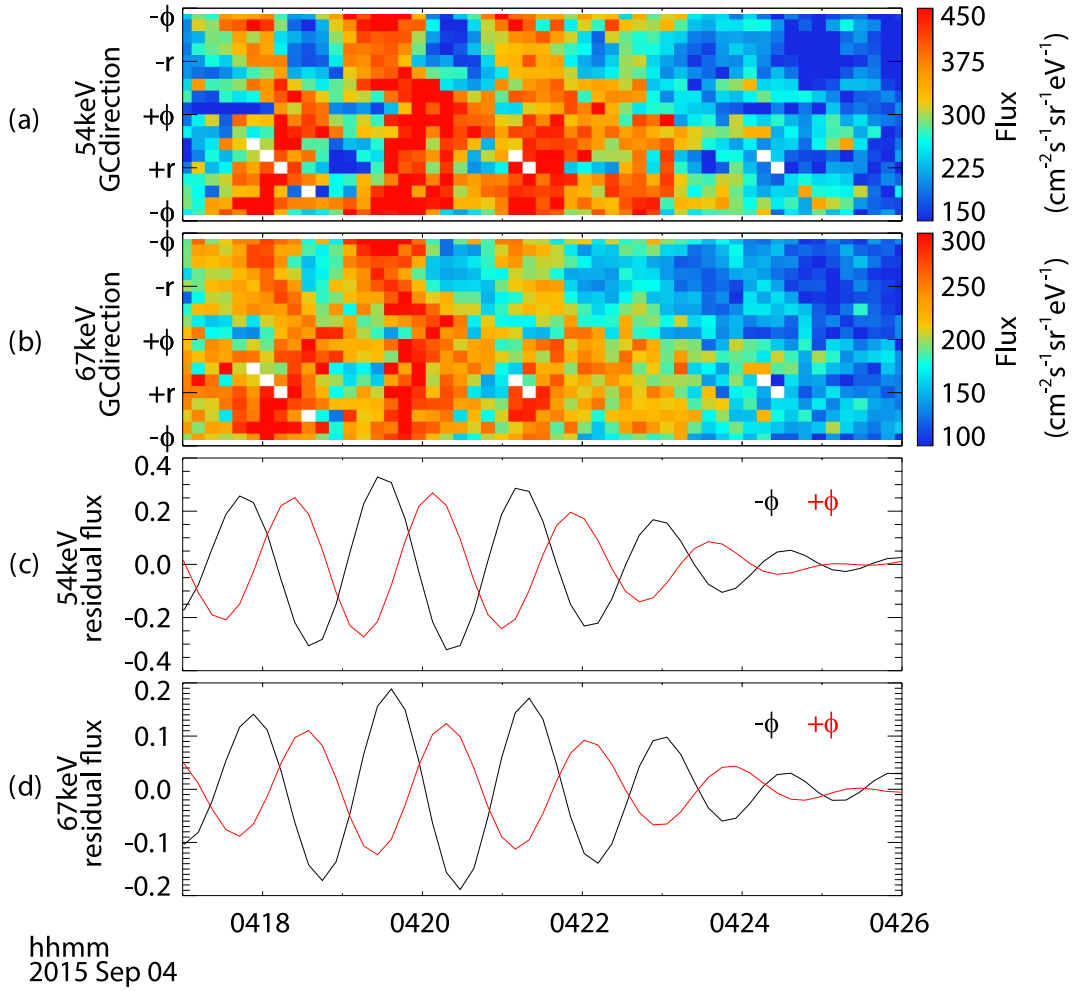

Figure 3. (a)–(b) Local 90° pitch angle proton fluxes in 54 keV (a) and 67 keV (b) as a function of the gyrocenter direction and time (c)–(d) The residual proton fluxes in the gyrocenter directions of $+\phi$ (red) and $-\phi$ (black) at 54 keV (c) and 67 keV (d).

$$|m| = \frac{\pi f \tau R_C}{\rho_G} \tag{8}$$

Figures 3c and 3d show the residual fluxes of local 90° pitch angle protons both in the $+\phi$ (depicted in red) and $-\phi$ (shown in black) directions with an 8–11 mHz band-pass filter. Employing cross-correlation analysis on these residual fluxes in opposite directions, we determined the τ for 54 and 67 keV proton residual fluxes are 32.0 and 41.4 s, respectively. The correlation coefficients for 54 and 67 keV protons are 0.98 and 0.99, respectively. Besides, the distance from Earth's center to the spacecraft (R_{sc}) is 4.64 R_E, the spacecraft latitude (λ_{sc}) is around 9.35°, and the wave frequency is estimated to be 10 mHz. By adopting these parameters in Equation 8, we derive the m value from the 54 and 67 keV proton observations to be 237 and 277, respectively. Thus, we determine the range of m value is 237–277.

2.3. The Excitation of ULF Waves

As shown in Figure 2, the resonant signatures are only seen at 54 and 67 keV, with the oscillations appearing more pronounced for protons at 54 keV. Therefore, we calculate the energy exchange between ULF waves and 54 keV protons. Besides, since the satellite is near the equator, there is only a 3° difference between the local resonant pitch angle and the equatorial resonant pitch angle, which is less than the observed pitch angle width. Thus, we use the local resonant pitch angle to represent the equatorial resonant pitch angle approximately.

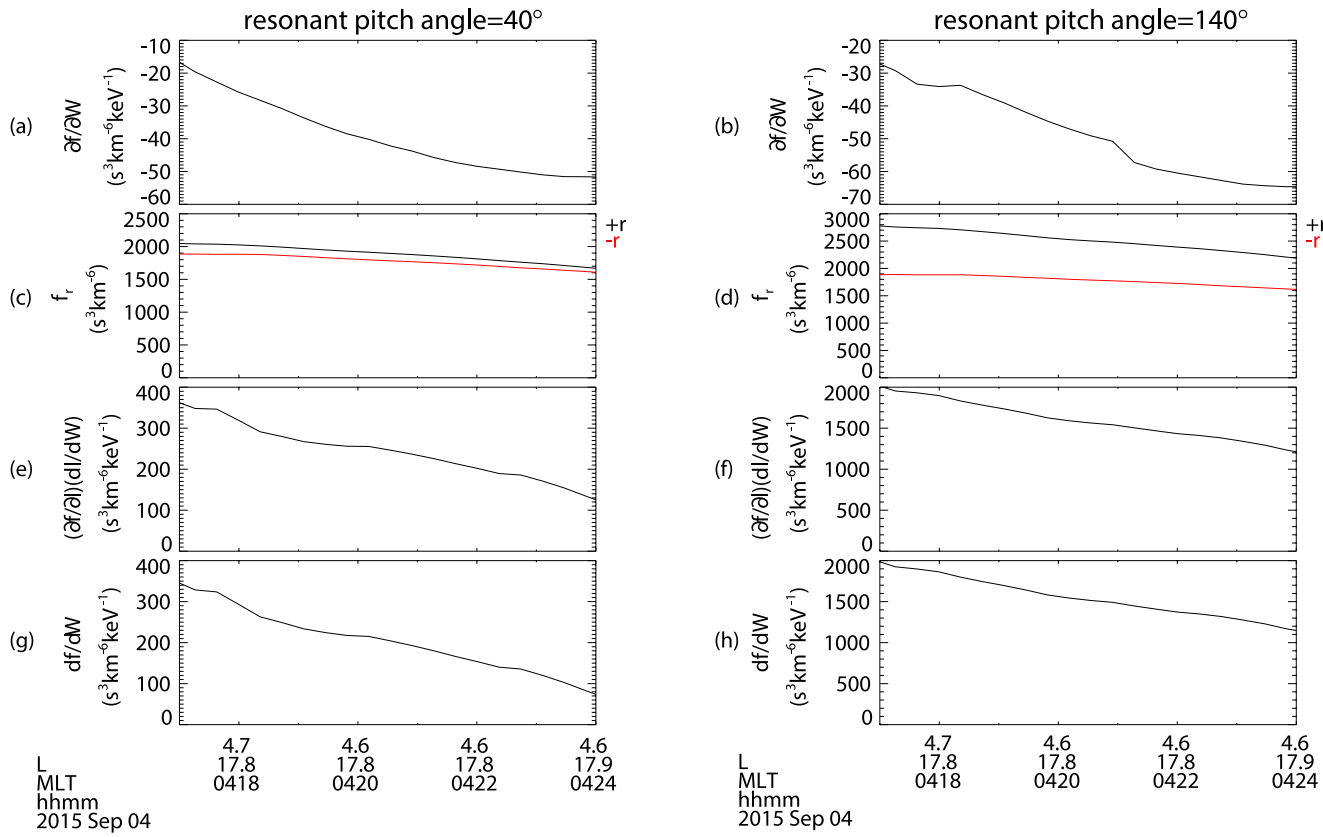

Figure 4. (a)–(b) The 54 keV proton phase space density (PSD) energy gradient for resonant pitch angles of 40° (a) and 140° (b) (c)–(d) The 54 keV proton phase space density with an outward gyrocenter (black) and an inward gyrocenter (red) for 40° (c) and 140° (d) resonant pitch angles (e)–(f) The radial gradient of 54 keV proton phase space density for 40° (e) and 140° (f) resonant pitch angles. (g)–(h) df/dW for 54 keV protons for resonant pitch angles of 40° (g) and 140° (h).

To determine whether waves are excited or damped through the drift-bounce resonance, we calculated each term in Equation 2. The averaged magnetic moment (μ_{res}) for 40° and 140° pitch angle protons at 54 keV is ~0.08 keV/nT. As depicted in Figures 4a and 4b, the energy gradients of PSD for both 40° and 140° pitch angle of 54 keV protons are negative, which stabilizes the plasma. Figures 4c and 4d reveal that the phase space density in the outward radial direction (+r, black line) is greater than the value in the inward direction (-r, red line). The distance between the two directions is twice as much as the Larmor radius of 54 keV protons. According to Southwood et al. (1969), we can obtain the ratio between changes in L and W for resonant particles as follows:

$$\frac{dL}{dW} = \frac{mL^2}{qB_E \omega R_E^2} \tag{9}$$

where m is the azimuthal wave number, L is the L shell, q is the electric charge of the particle, and B_E is the magnitude of equatorial magnetic field on the surface of the Earth. We use the parameter $m = 237$ (the minimum value of the m range) and $\omega = 0.0628$ rad/s. By multiplying $\frac{dL}{dW}$ and $\frac{\partial f}{\partial L}$, we obtained the minimum value of the second term in Equation 2 for 54 keV protons, which is shown in Figures 4e and 4f. Combining the positive $\frac{dL}{dW}\frac{\partial f}{\partial L}$ and the negative energy gradient, we determined that $\frac{df}{dW}$ is indeed positive, which indicates the ULF waves are excited by the protons inside the magnetic dip.

3. Summary and Discussion

In this study, we have analyzed an observational event, which provides evidence for the excitation of ULF waves by energetic protons inside a magnetic dip. On 4 September 2015, RBSP-B encountered a magnetic dip during a strong substorm with an SME_{max} index of approximately 1,000 nT. It was also in the main phase of a weak storm

with a minimum SYM-H index of ∼−50 nT, and there was no solar wind dynamic pressure enhancement before this event. ULF signals were detected inside the magnetic dip. Unfortunately, RBSP-A was in the inner belt and thus missed the event. Besides, no other satellite observed similar ULF signals, and the ground magnetometers didn't detect these waves because of ionospheric screening effects (Hughes & Southwood, 1976). Further investigation shows that the ULF waves are second harmonic poloidal waves with a period of ∼100 s. The quasi-periodic oscillations of omniflux and a series of curved stripes in pitch angle-time spectrograms with the same period of ULF waves for 54 and 67 keV protons reveal the drift-bounce resonance between protons and ULF waves, and the oscillations appear more pronounced for protons at 54 keV. The 180° phase shifts across 40°/140° in observation further indicates the resonant pitch angle is 40°/140°.

Since there is only one satellite observation, the propagation direction of the ULF waves is obtained through finite Larmor radius effects. The protons whose gyrocenters are located westward of the spacecraft are affected by the waves first, indicating that the wave is propagating eastward. The range of the azimuthal wave number (m) is derived through the phase delay between fluxes in the $+\phi$ and $-\phi$ directions. For 54 and 67 keV protons, the obtained m values are 237 and 277, respectively. It's worth noting that the interpolation of residual fluxes into 0.1-s intervals introduced a degree of error into the time delay calculations.

The energy transfer direction is derived by determining the sign of $\frac{df}{dW}$. For 54 keV protons with the resonant pitch angle of 40°/140°, the energy gradient of PSD is negative while $\frac{dL}{dW}\frac{\partial f}{\partial L}$ is positive. Combining the two terms, we derive that the $\frac{df}{dW} > 0$, which indicates that the ULF waves are excited through drift-bounce resonance with energetic protons in the magnetic dip.

In our study, the drift-bounce resonance is restricted in the magnetic dip. Here, we attempt to give a possible explanation about the effect of magnetic dip on the drift-bounce resonance. During substorms, injections lead to simultaneous enhancements in phase space density across different energies, and the diamagnetic motion of injected particles produces a magnetic dip. After that, these particles drift around the Earth, displaying dispersive features. The magnetic dip, in turn, can slow the drift speed of the protons down by altering the radial gradient of the magnetic fields. The slower drift speed tends to group protons of 10s keV (major energy range to significantly contribute plasma pressure) together, enhancing the local phase space density and providing free energy to excite ULF waves in the magnetic dip. In our case, the drift-bounce resonance occurs in 17.8–17.9 MLT, which is outside the dispersionless injection region. If the effect of the magnetic dip is not considered, assuming a dipole field, the protons with different energies and pitch angles would separate each other following the drift speed of $\omega_d = -\frac{6WL}{qB_E R_E^2}(0.35 + 0.15 \sin \alpha_{eq})$ (Hamlin et al., 1961). Here, W is the particle's energy, L is the L shell, B_E is the equatorial magnetic field on Earth's surface, R_E is Earth's radius, and α_{eq} is the particle's equatorial pitch angle. For example, the drift speed of 54 keV protons of 40° pitch angle is 7.4 MLT/hr. However, in the presence of the magnetic dip, the formula of drift speed in the dipole fields is no longer applicable. Despite this, the drift speed for resonant protons can be obtained through the drift-bounce resonance condition $\omega - m\omega_d = N\omega_b$. We have obtained the frequency (ω) is 10 mHz, and the m number is in the range of 237–277 for the observed ULF waves through finite Larmor radius effects. Since the observed second harmonic ULF waves propagate eastward, $N = 1$. The bounce frequency can be calculated using the formula $\omega_b = \frac{\pi\sqrt{2W/M}}{2LR_E(1.30 - 0.56 \sin \alpha_{eq})}$ (Hamlin et al., 1961), where W is the particle's energy, M is the particle mass, L is the L shell, R_E is Earth's radius, and α_{eq} is the particle's equatorial pitch angle. With the parameters above, the drift speed for the resonant 54 keV protons with a 40° pitch angle in the magnetic dip is found to be 5.9–6.9 MLT/hr, which is lower than their drift speed (7.4 MLT/hr) in dipole fields. Similarly, the drift speed for the resonant 67 keV protons with a 40° pitch angle in the magnetic dip is 7.0–8.2 MLT/hr, compared to 9.2 MLT/hr in dipole fields. As a result, protons in the magnetic dip drift more slowly and tend to group together, enhancing the local phase space density and providing free energy to excite ULF waves in the magnetic dip.

Our study provides a clear observation of internally driven ULF waves through drift-bounce resonance. Previous studies have also mentioned ring current protons could excite ULF waves through drift-bounce resonance (Min et al., 2017; Yamamoto et al., 2019), but none of them are related to the magnetic dip structure. Our study proposes for the first time that the magnetic dip provides a new source to generate ULF waves. We summarize the key findings as follows.

1. During a substorm ($SME_{max} \sim 1000$ nT), RBSP-B encountered a magnetic dip at the dusk side. Inside the magnetic dip, the fields oscillate quasi-periodically, and the protons from 54 to 67 keV exhibit drift-bounce resonance with ULF waves.
2. The ULF waves are diagnosed as Pc 4 second harmonic poloidal waves.
3. Through finite Larmor radius effects, the ULF waves are found to propagate eastward with the azimuthal wave number of 237–277.
4. The sign of df/dW is positive. Thus, we determine that drift-bounce resonance excites eastward second harmonic poloidal ULF waves with a high m number. The excitation of ULF waves is related to the enhancement of energetic proton phase space densities in the magnetic dip.

Data Availability Statement

We acknowledge the use of Van Allen Probes data, such as ToFxEH (https://cdaweb.gsfc.nasa.gov/pub/data/rbsp/rbspb/l3/rbspice/tofxeh/) and PAP_ToFxEH (https://cdaweb.gsfc.nasa.gov/pub/data/rbsp/rbspb/l3/rbspice/pap_tofxeh/) RBSPICE particle flux data; level 3 EMFISIS data from https://emfisis.physics.uiowa.edu/data/index, level 2 EMF data available at http://www.space.umn.edu/rbspefw-data/.

Acknowledgments
The study is supported by NSFC research Grants 42274200 and National Key R&D Program of China 2023YFC2808900.

References

Birn, J., Thomsen, M. F., Borovsky, J. E., Reeves, G. D., McComas, D. J., & Belian, R. D. (1997). Characteristic plasma properties during dispersionless substorm injections at geosynchronous. *Orbit*, *102*(A2), 2309–2324. https://doi.org/10.1029/96JA02870

Chen, Z., Su, Z., He, Z., Wu, Z., Dai, G., Wang, B., et al. (2022). A rapid localized deceleration of Earth's radiation belt relativistic electrons driven by storm. *Proton Injection*, *49*(9), e2022GL098810. https://doi.org/10.1029/2022GL098810

Claudepierre, S. G., Elkington, S. R., & Wiltberger, M. (2008). Solar wind driving of magnetospheric ULF waves: Pulsations driven by velocity shear at the magnetopause. *Journal of Geophysical Research*, *113*(A5), A05218. https://doi.org/10.1029/2007JA012890

Ebihara, Y., Fok, M.-C., Blake, J. B., & Fennell, J. F. (2008). Magnetic coupling of the ring current and the radiation belt. *Journal of Geophysical Research*, *113*(A7), A07221. https://doi.org/10.1029/2008JA013267

Glassmeier, K. H., Buchert, S., Motschmann, U., Korth, A., & Pedersen, A. (1999). Concerning the generation of geomagnetic giant pulsations by drift-bounce resonance ring current instabilities. *Annals of Geophysics*, *17*(3), 338–350. https://doi.org/10.1007/s00585-999-0338-4

Grinsted, A., Moore, J. C., & Jevrejeva, S. (2004). Application of the cross wavelet transform and wavelet coherence to geophysical time series. *Nonlinear Processes in Geophysics*, *11*(5/6), 561–566. https://doi.org/10.5194/npg-11-561-2004

Hamlin, D. A., Karplus, R., Vik, R. C., & Watson, K. M. (1961). Mirror and azimuthal drift frequencies for geomagnetically trapped particles. *Journal of Geophysical Research*, *66*(1), 1–4. https://doi.org/10.1029/JZ066i001p00001

Hao, Y. X., Zong, Q., Wang, Y. F., Zhou, X., Zhang, H., Fu, S. Y., et al. (2014). Interactions of energetic electrons with ULF waves triggered by interplanetary shock. *Van Allen Probes observations in the magnetotail*, *119*(10), 8262–8273. https://doi.org/10.1002/2014JA020023

He, Z., Chen, L., Zhu, H., Xia, Z., Reeves, G. D., Xiong, Y., et al. (2017). Multiple-satellite observation of magnetic dip event during the substorm. *Geophysical Research Letters*, *44*(18), 9167–9175. https://doi.org/10.1002/2017GL074869

Huang, Z., Yuan, Z., Yu, X., Xue, Z., & Ouyang, Z. (2021). Simultaneous generation of EMIC and MS waves during the magnetic dip in the inner magnetosphere. *Geophysical Research Letters*, *48*(18), e2021GL094842. https://doi.org/10.1029/2021GL094842

Hughes, W. J., McPherron, R. L., & Barfield, J. N. (1978). Geomagnetic pulsations observed simultaneously on three geostationary satellites. *Journal of Geophysical Research*, *83*(A3), 1109–1116. https://doi.org/10.1029/JA083iA03p01109

Hughes, W. J., & Southwood, D. J. (1976). An illustration of modification of geomagnetic pulsation structure by the ionosphere. *Journal of Geophysical Research*, *81*(19), 3241–3247. https://doi.org/10.1029/JA081i019p03241

Kivelson, M. G., & Southwood, D. J. (1983). Charged particle behavior in low-frequency geomagnetic pulsations: 3. *Spin phase dependence*, *88*(A1), 174–182. https://doi.org/10.1029/JA088iA01p00174

Kletzing, C. A., Kurth, W. S., Acuna, M., MacDowall, R. J., Torbert, R. B., Averkamp, T., et al. (2013). The electric and magnetic field instrument suite and integrated science (EMFISIS) on RBSP. *Space Science Reviews*, *179*(1), 127–181. https://doi.org/10.1007/s11214-013-9993-6

Li, L., Zhou, X., Omura, Y., Zong, Q., Liu, Y., Rankin, R., et al. (2024). Nonlinear drift-bounce resonance between charged particles and ultralow frequency waves. *Journal of Geophysical Research: Space Physics*, *129*(8), e2024JA032742. https://doi.org/10.1029/2024JA032742

Li, Y.-X., Yue, C., Ma, Q., Liu, J., Zong, Q., Zhou, X., et al. (2022). Simultaneous cross-energy ion response and wave generation after the impact of an interplanetary shock. *Journal of Geophysical Research: Space Physics*, *127*(11), e2022JA030636. https://doi.org/10.1029/2022JA030636

Lin, N., McPherron, R. L., Kivelson, M. G., & Williams, D. J. (1988). An unambiguous determination of the propagation of a compressional Pc 5 wave. *Journal of Geophysical Research*, *93*(A6), 5601–5612. https://doi.org/10.1029/JA093iA06p05601

Liu, W., Cao, J. B., Li, X., Sarris, T. E., Zong, Q.-G., Hartinger, M., et al. (2013). Poloidal ULF wave observed in the plasmasphere boundary layer. *Journal of Geophysical Research: Space Physics*, *118*(7), 4298–4307. https://doi.org/10.1002/jgra.50427

Liu, Z.-Y., Zong, Q.-G., Zhou, X.-Z., Zhu, Y.-F., & Gu, S.-J. (2020). Pitch angle structures of ring current ions induced by evolving poloidal ultra-low frequency waves. *Geophysical Research Letters*, *47*(4), e2020GL087203. https://doi.org/10.1029/2020GL087203

Mauk, B. H., Fox, N. J., Kanekal, S. G., Kessel, R. L., Sibeck, D. G., & Ukhorskiy, A. (2013). Science objectives and rationale for the radiation belt storm probes mission. *Space Science Reviews*, *179*(1), 3–27. https://doi.org/10.1007/s11214-012-9908-y

McIlwain, C. E. (1961). Coordinates for mapping the distribution of magnetically trapped particles. *Journal of Geophysical Research*, *66*(11), 3681–3691. https://doi.org/10.1029/JZ066i011p03681

Min, K., Takahashi, K., Ukhorskiy, A. Y., Manweiler, J. W., Spence, H. E., Singer, H., et al. (2017). Second harmonic poloidal waves observed by Van Allen Probes in the dusk-midnight sector. *Journal of Geophysical Research: Space Physics*, *122*(3), 3013–3039. https://doi.org/10.1002/2016JA023770

Mitchell, D. G., Lanzerotti, L. J., Kim, C. K., Stokes, M., Ho, G., Cooper, S., et al. (2013). Radiation belt storm probes ion composition experiment (RBSPICE). *Space Science Reviews*, *179*(1), 263–308. https://doi.org/10.1007/s11214-013-9965-x

Motoba, T., Ohtani, S., Gkioulidou, M., Ukhorskiy, A. Y., Lanzerotti, L. J., & Claudepierre, S. G. (2021). Superposed epoch analysis of dispersionless particle injections inside geosynchronous. *Orbit*, *126*(8), e2021JA029546. https://doi.org/10.1029/2021JA029546

Ozeke, L. G., & Mann, I. R. (2008). Energization of radiation belt electrons by ring current ion driven ULF waves. *Journal of Geophysical Research*, *113*(A2), A02201. https://doi.org/10.1029/2007JA012468

Rankin, R., Wang, C. R., Wang, Y. F., Zong, Q., Zhou, X. Z., Degeling, A. W., et al. (2020). Ultra-Low-frequency wave–particle interactions in Earth's outer radiation belt. *Dayside Magnetosphere Interactions*, 189–205. https://doi.org/10.1002/9781119509592.ch11

Ren, J., Zong, Q. G., Zhou, X. Z., Rankin, R., & Wang, Y. F. (2016). Interaction of ULF waves with different ion species: Pitch angle and phase space density implications. *Journal of Geophysical Research: Space Physics*, *121*(10), 9459–9472. https://doi.org/10.1002/2016JA022995

Singer, H. J., Hughes, W. J., & Russell, C. T. (1982). Standing hydromagnetic waves observed by ISEE 1 and 2: Radial extent and harmonic. *Journal of Geophysical Research*, *87*(A5), 3519–3529. https://doi.org/10.1029/JA087iA05p03519

Southwood, D. J., Dungey, J. W., & Etherington, R. J. (1969). Bounce resonant interaction between pulsations and trapped particles. *Planetary and Space Science*, *17*(3), 349–361. https://doi.org/10.1016/0032-0633(69)90068-3

Southwood, D. J., & Hughes, W. J. (1983). Theory of hydromagnetic waves in the magnetosphere. *Space Science Reviews*, *35*(4), 301–366. https://doi.org/10.1007/BF00169231

Southwood, D. J., & Kivelson, M. G. (1981). Charged particle behavior in low-frequency geomagnetic pulsations 1. *Transverse waves*, *86*(A7), 5643–5655. https://doi.org/10.1029/JA086iA07p05643

Su, S.-Y., Konradi, A., & Fritz, T. A. (1977). On propagation direction of ring current proton ULF waves observed by ATS 6 at 6.6 RE. *Journal of Geophysical Research*, *82*(13), 1859–1868. https://doi.org/10.1029/JA082i013p01859

Takahashi, K., Oimatsu, S., Nosé, M., Min, K., Claudepierre, S. G., Chan, A., et al. (2018). Van Allen probes observations of second harmonic poloidal standing Alfvén waves. *Journal of Geophysical Research: Space Physics*, *123*(1), 611–637. https://doi.org/10.1002/2017JA024869

Thébault, E., Finlay, C. C., Beggan, C. D., Alken, P., Aubert, J., Barrois, O., et al. (2015). International geomagnetic reference field: The 12th generation. *Earth Planets and Space*, *67*(1), 79. https://doi.org/10.1186/s40623-015-0228-9

Wygant, J. R., Bonnell, J. W., Goetz, K., Ergun, R. E., Mozer, F. S., Bale, S. D., et al. (2013). The electric field and waves instruments on the radiation belt storm probes mission. *Space Science Reviews*, *179*(1), 183–220. https://doi.org/10.1007/s11214-013-0013-7

Xie, Z.-K., Zong, Q. G., Ren, J., Yue, C., Liu, Z., Liu, J., et al. (2023). Global ULF waves excited by solar wind dynamic pressure impulses: 1. *Timescales and Geomagnetic Activity Dependence*, *128*(10), e2023JA031813. https://doi.org/10.1029/2023JA031813

Xiong, Y., Chen, L., Xie, L., Fu, S., Xia, Z., & Pu, Z. (2017). Relativistic electron's butterfly pitch angle distribution modulated by localized background magnetic field perturbation driven by hot ring current ions. *Geophysical Research Letters*, *44*(10), 4393–4400. https://doi.org/10.1002/2017GL072558

Yamamoto, K., Nosé, M., Kasahara, S., Yokota, S., Keika, K., Matsuoka, A., et al. (2018). Giant pulsations excited by a steep earthward gradient of proton phase space density: Arase. *Observation*, *45*(14), 6773–6781. https://doi.org/10.1029/2018GL078293

Yamamoto, K., Nosé, M., Keika, K., Hartley, D. P., Smith, C. W., MacDowall, R. J., et al. (2019). Eastward propagating second harmonic poloidal waves triggered by temporary outward gradient of proton phase space density: Van Allen probe A. *Observation*, *124*(12), 9904–9923. https://doi.org/10.1029/2019JA027158

Yan, Y., Yue, C., Yin, Z.-F., Zhou, X.-Z., Zong, Q.-G., & Li, J.-H. (2023). Amplitude-dependent properties and excitation mechanisms of EMIC waves in the. *Earth's Inner Magnetosphere*, *128*(7), e2023JA031451. https://doi.org/10.1029/2023JA031451

Yang, B., Zong, Q.-G., Fu, S. Y., Li, X., Korth, A., Fu, H. S., et al. (2011). The role of ULF waves interacting with oxygen ions at the outer ring current during storm times. *Journal of Geophysical Research*, *116*(A1), A01203. https://doi.org/10.1029/2010JA015683

Yin, Z.-F., Zhou, X., Hu, Z., Yue, C., Zong, Q., Hao, Y., et al. (2022). Localized excitation of electromagnetic ion cyclotron waves from anisotropic protons filtered by magnetic dips. *Journal of Geophysical Research: Space Physics*, *127*(6), e2022JA030531. https://doi.org/10.1029/2022JA030531

Yin, Z.-F., Zhou, X.-Z., Zong, Q.-G., Liu, Z.-Y., Yue, C., Xiong, Y., et al. (2021). Inner magnetospheric magnetic dips and energetic protons trapped therein: Multi-spacecraft observations and simulations. *Geophysical Research Letters*, *48*(7), e2021GL092567. https://doi.org/10.1029/2021GL092567

Yue, C., Jun, C., Bortnik, J., An, X., Ma, Q., Reeves, G. D., et al. (2019). The relationship between EMIC wave properties and proton distributions based on van Allen probes observations. *Geophysical Research Letters*, *46*(8), 4070–4078. https://doi.org/10.1029/2019GL082633

Zhang, D., Liu, W., Li, X., Sarris, T. E., Wang, Y., Xiao, C., et al. (2020). Relation between shock-related impulse and subsequent ULF wave in the. *Earth's Magnetosphere*, *47*(23), e2020GL090027. https://doi.org/10.1029/2020GL090027

Zhao, Y., Zhu, H., & Chen, H. (2023). Expected EMIC wave generation and unexpected MS wave disruption in a magnetic dip. *Journal of Geophysical Research: Space Physics*, *128*(8), e2023JA031776. https://doi.org/10.1029/2023JA031776

Zhu, H., Chen, L., Artemyev, A. V., Zhang, X.-J., & Breneman, A. W. (2021). Superposed epoch analyses of electron-driven and proton-driven magnetic dips. *Geophysical Research Letters*, *48*(21), e2021GL094934. https://doi.org/10.1029/2021GL094934

Zhu, Y.-F., Gu, S.-J., Zhou, X.-Z., Zong, Q.-G., Ren, J., Sun, X.-R., et al. (2020). Drift-bounce resonance between charged particles and ultralow frequency waves: Theory and observations. *Journal of Geophysical Research: Space Physics*, *125*(1), e2019JA027067. https://doi.org/10.1029/2019JA027067

Zhuang, Y., Yue, C., Zong, Q.-G., Zhou, X.-Z., Fu, H., Mitchell, D. G., et al. (2023). The effect of energetic ion dispersionless injections on the ring. *Current Dynamics*, *128*(2), e2022JA030914. https://doi.org/10.1029/2022JA030914

Zong, Q. (2022). Magnetospheric response to solar wind forcing: Ultra-low-frequency wave–particle interaction perspective. *Annals of Geophysics*, *40*(1), 121–150. https://doi.org/10.5194/angeo-40-121-2022

Zong, Q., Rankin, R., & Zhou, X. (2017). The interaction of ultra-low-frequency pc3-5 waves with charged particles in Earth's magnetosphere. *Reviews of Modern Plasma Physics*, *1*(1), 10. https://doi.org/10.1007/s41614-017-0011-4

Zong, Q.-G., Wang, Y. F., Zhang, H., Fu, S. Y., Zhang, H., Wang, C. R., et al. (2012). Fast acceleration of inner magnetospheric hydrogen and oxygen ions by shock induced ULF waves. *Journal of Geophysical Research*, *117*(A11), A11206. https://doi.org/10.1029/2012JA018024

Zong, Q.-G., Zhou, X.-Z., Wang, Y. F., Li, X., Song, P., Baker, D. N., et al. (2009). Energetic electron response to ULF waves induced by interplanetary shocks in the outer radiation belt. *Journal of Geophysical Research*, *114*(A10), A10204. https://doi.org/10.1029/2009JA014393

Erratum

The originally published version of this article contained typographical errors. In Equation 2, the first expression "ddf" should be changed to df. In item 2 of the list at the end of Section 3, "s harmonic" should be changed to "second harmonic." The errors have been corrected, and this may be considered the authoritative version of record.